AGU PUBLICATIONS

JGR

Journal of Geophysical Research: Solid Earth

RESEARCH ARTICLE

10.1002/2016JB013081

Velocity-weakening behavior of Westerly granite at temperature up to 600°C

E. K. Mitchell[1], Y. Fialko[1], and K. M. Brown[1]

[1] Institute of Geophysics and Planetary Physics, Scripps Institution of Oceanography, University of California, San Diego, La Jolla, California, USA

Key Points:
- New experimental data reveal velocity-weakening behavior of Westerly granite up to 600°C
- At high (>400°C) temperature, the effect of pore pressure on rate dependence of friction is inferred to be highly nonlinear
- New data may be relevant to deep crustal seismicity and dynamic weakening during seismic rupture

Supporting Information:
- Supporting Information S1

Correspondence to:
Y. Fialko,
yfialko@ucsd.edu

Citation:
Mitchell, E. K., Y. Fialko, and K. M. Brown (2016), Velocity-weakening behavior of Westerly granite at temperature up to 600°C, *J. Geophys. Res. Solid Earth*, *121*, 6932–6946, doi:10.1002/2016JB013081.

Received 10 APR 2016
Accepted 24 AUG 2016
Accepted article online 26 AUG 2016
Published online 27 SEP 2016

Abstract The deep limit to seismicity in continental crust is believed to be controlled by a transition from velocity-weakening to velocity-strengthening friction based on experimental measurements of the rate dependence of friction at different temperatures. Available experimental data on granite suggest a transition to stable creep at about 350°C (~15 km depth). Here we present results from unconfined experiments on Westerly granite at both dry and hydrated conditions that show increasingly unstable slip (velocity-weakening behavior) at temperature up to 600°C. A comparison of previously published experimental results with those presented in this study suggests that the rate and state friction parameters strongly depend on normal stress and pore pressure at high (>400°C) temperature, which may help explain regional variations in the depth distribution of earthquakes in continental crust. Temperature dependence of the rate and state friction parameters may also contribute to strong dynamic weakening observed in high-speed friction experiments on crystalline rocks such as granite and gabbro.

1. Introduction

Most earthquakes in the continental lithosphere occur in the upper crust [*Eaton et al.*, 1970; *Hill et al.*, 1975; *Sibson*, 1982]. Termination of seismicity at depth of 12–15 km is usually attributed to a transition from velocity-weakening to velocity-strengthening friction [*Tse and Rice*, 1986; *Marone*, 1998]. Indeed, laboratory measurements of the dependence of friction on slip rate for Westerly granite (a rock type widely used in experimental studies as a material representative of the upper crust) showed a transition from velocity-weakening behavior (conditionally unstable slip) to velocity-strengthening behavior (stable creep) at temperatures above 300–350°C [*Stesky*, 1978; *Blanpied et al.*, 1991, 1995]. Assuming a typical geotherm of 20–25°C/km [e.g., *Nathenson and Guffanti*, 1988], this transition is expected to occur at depth of ~12–17 km, in good agreement with the depth distribution of earthquakes in California [*Marone and Scholz*, 1988; *Blanpied et al.*, 1991; *Nazareth and Hauksson*, 2004]. The temperature dependence of slip stability is believed to control the depth range of seismicity, as earthquakes would not be able to nucleate under velocity-strengthening conditions [*Brace and Byerlee*, 1966; *Dieterich*, 1974; *Ruina*, 1983]. Recent observations, however, indicate that the middle and lower continental crust can host slip instabilities in the form of regular earthquakes [*Jackson*, 2002; *Emmerson et al.*, 2006; *Leyton et al.*, 2009; *Craig et al.*, 2011; *Inbal et al.*, 2015] and tremor [*Shelly*, 2010; *Trugman et al.*, 2015] at temperatures above 300–350°C at which existing laboratory data would imply stable creep.

Most of the high-temperature tests on Westerly granite were performed using the same type of experimental apparatus, triaxial machine [*Stesky*, 1978; *Lockner et al.*, 1986; *Blanpied et al.*, 1991]. *Mitchell et al.* [2013] used a direct shear apparatus to study the dependence of frictional healing of Westerly granite on temperature. Somewhat surprisingly, they observed unstable slip at temperature up to 450°C. Experiments of *Mitchell et al.* [2013] were limited to solid samples (bare surfaces with small amount of gouge generated during the experiments), relatively low normal stress (5 MPa) and dry conditions. Here we report results of direct shear experiments on Westerly granite conducted over a wider range of conditions including temperatures between 20 and 600°C, load point velocities 10^{-5} to 3×10^{-2} mm/s, normal stresses 5–40 MPa, on bare surfaces and thick gouge, on dry samples, and in the presence of water. We find that parameter $(a - b)$ that characterizes dependence of friction on slip rate [*Dieterich*, 1979; *Ruina*, 1983] becomes increasingly more negative with temperature over the entire temperature range under all tested conditions. We discuss possible reasons for different results obtained in direct shear and triaxial experiments, and implications for constitutive laws describing rate dependence of friction, and observations of deep seismicity in continental crust.

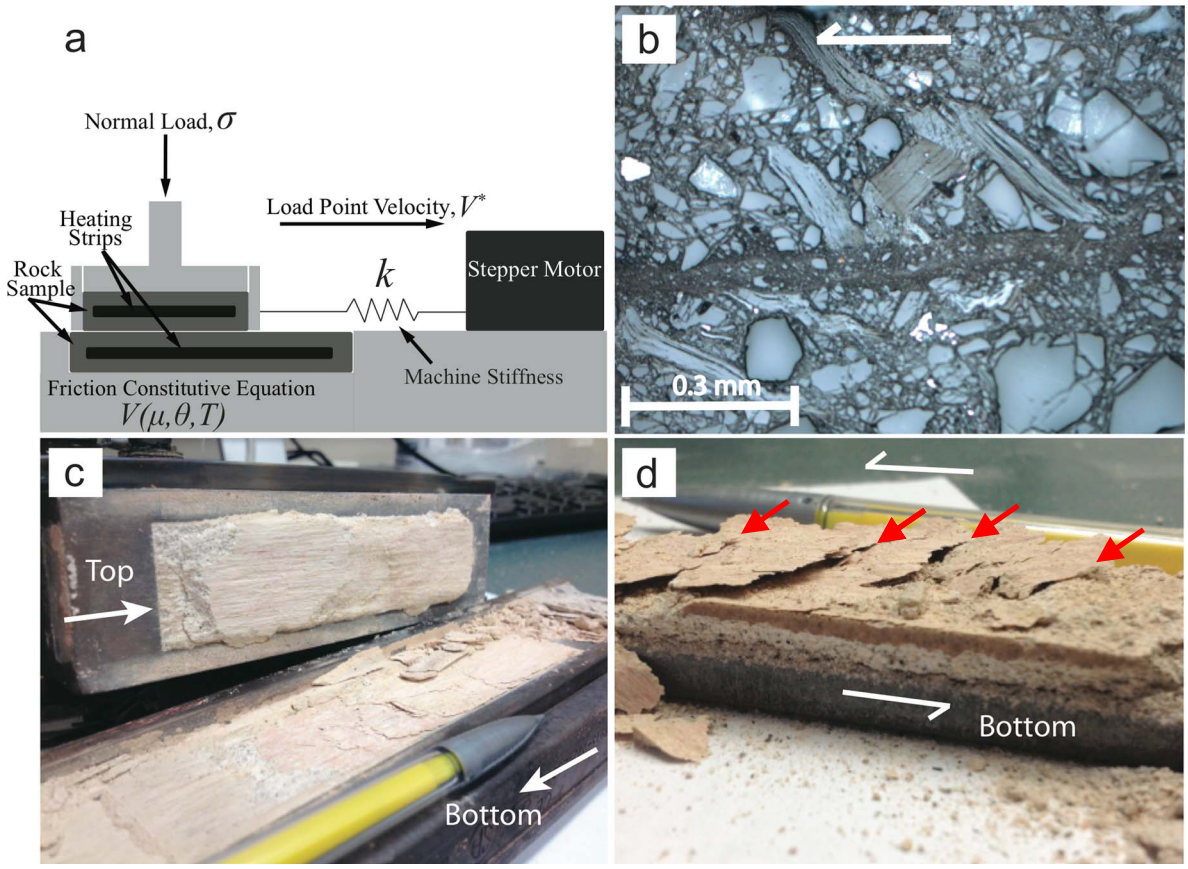

Figure 1. Experimental setup. (a) Diagram of the heated direct shear apparatus. (b) Microscope image of a thin section of the gouge sample, plane light. Arrow indicates the shear direction. Reduced grain size can be seen within the shear zone. Note sheared grains of biotite and crushed grains of feldspar. (c) Photograph of the top and bottom halves of the gouge sample within the sample holders. The sample separated along the primary slip surface. (d) Bottom half of the gouge sample after removal from the sample holder. White arrows indicate shear direction. Grain size is dramatically reduced toward the primary slip surface. Red arrows indicate Riedel shear zones. Sample from test d216-77.

2. Experimental Setup and Procedure

The direct shear apparatus used in this study is schematically illustrated in Figure 1a. The apparatus has a stiffness of 9 MPa/mm, and a contact area between rock samples of 2.64×10^3 mm^2. The steel sample holders have a rectangular geometry and are positioned horizontally so that the shorter sample rests on top of the longer one. The temperature is measured using a thermocouple inserted in the sample within several millimeters from the slip interface. A constant temperature is maintained by controlling power supply to electric strip heaters connected to the sample holders. A thermal insulation is built around the sample holders and strip heaters to minimize heat loss to the surrounding medium. Normal stress is applied to the top sample holder by a ram with a proportional-integral-derivative (PID)-controlled hydraulic pump accurate to ~0.1 MPa. The ram moves sideways together with the top sample along low friction rails. The top sample is pulled horizontally using a stepper motor. The horizontal load point velocity is applied as close as possible to the slip interface to reduce rocking or torquing around the shear interface. To quantify the amount of tilt of the top sample holder we performed several cycles of loading and unloading and registered reversible displacements. The contribution of tilt to the displacement data was found to be 0.03 mm/MPa for shear stress up to 15 MPa, and 0.05 mm/MPa for shear stress greater than 15 MPa. The respective contributions were removed from the displacement time series.

Solid samples of the Westerly granite (10 mm thick, 25 mm wide, and 80–120 mm long) were prepared by grinding to a flatness of 4 μm/m and roughness of grit #80. The simulated gouge samples were prepared by crushing solid blocks of Westerly granite using a sledge hammer and sorting through a sieve with 1.67 mm holes. The initial thickness of the gouge samples was 15 mm. The samples were compressed at 30 MPa normal

stress and compacted to a thickness of about 9 mm. Gouge samples were sheared using rough driving plates at the top and the bottom of the sample holder. Shear stress, displacement, and normal stress were recorded at a rate of 10 samples per second per channel. In several high-temperature experiments data were recorded at sampling rates in excess of 1000 samples per second to resolve the maximum velocity during slip events.

The maximum slip distance in a single test is 40 mm. Much larger total displacements can be achieved upon resetting the sample multiple times (e.g., by reducing the normal stress and moving the ram back to the original position), although this may result in some disruption of shear fabric. Friction coefficient was computed by dividing the measured shear stress by the measured normal stress at every time sample. We found that the dependence of friction coefficient on total displacement is most prominent in the initial ~20 mm of slip. Most of the experiments presented here were conducted after an initial run-in over distance of 160 mm. Some of the tests produced a small systematic trend in shear stress. This is not unusual in friction experiments, possibly due to slight irregularities of the slip interface, development of shear fabric, and/or piling of gouge at the leading edge of a moving sample. In such cases, a best fitting linear trend T was removed from the time series of stress. The estimated values of T are indicated in captions for figures that display the measured shear stress or coefficient of friction.

In tests done at low (20–150°C) temperatures, the samples were held at 200°C for an hour and allowed to cool down to the desired temperature to reduce the effects of room humidity on friction and to allow a direct comparison between dry tests performed at various temperatures.

A relatively low stiffness of the direct shear apparatus allows for unstable sliding (stick slip). Stick-slip behavior is an unambiguous indicator of velocity-weakening friction [*Ruina*, 1983; *Heslot et al.*, 1994]. In cases of stable or quasi-stable slip, we performed velocity-stepping tests and directly measured the rate and state friction parameters a, b, D_c, and μ_o to verify the effect of temperature on rate dependence of friction, and to provide independent constraints on the values of the rate and state parameters inferred from numerical simulations, as described in section 3. The measured values of individual parameters a and b in velocity-stepping tests are likely lower bounds because of a finite stiffness of the experimental apparatus [e.g., *Nakatani*, 2001]. However, the values of $(a - b)$ should be robust as they are evaluated at steady state. At temperatures greater than 400°C, slip is unstable, and the samples exhibit episodic accelerated creep or stick slip. In case of unstable slip, the rate and state parameters were inferred from numerical models that provided best fit to the stress time series, as described in section 3.

To investigate the effects of water, we performed a series of tests under hydrated conditions. In these tests the water was injected at the bottom of the sample holder at constant flow rate of 2 mL/min and a pressure cap of 0.7 MPa using a syringe pump. Because the sample is unconfined, the water flashed to vapor under high-temperature conditions (note that in confined experiments, water is expected to be in a supercritical state, so there is no distinction between liquid and vapor [*Franck*, 1983]).

We also conducted a series of slide-hold-slide tests on gouge samples of Westerly granite to investigate the effect of temperature on frictional healing (Figure S1 in the supporting information). Slide-hold-slide tests provide a measure of the evolution parameter, b, that is independent from results of velocity-stepping tests and parameter fitting using spring-slider models. The rate of frictional healing can be calculated as $b = \mathrm{d}\mu_p/\mathrm{dln}(t_h)$ [e.g., *Beeler et al.*, 1994; *Mitchell et al.*, 2013], where μ_p is static coefficient of friction and t_h is the hold time. We find that b is nearly zero at room temperature and increases with temperature up to ~0.01 at 600°C. These estimates for b are in general agreement with those inferred from velocity-stepping tests (Figure 5b) and with results reported by *Mitchell et al.* [2013] for solid samples of Westerly granite. Table 1 provides a summary of loading conditions for all experiments used in this study.

3. Numerical Modeling of Unstable Slip

Data from experiments that exhibited time-dependent sliding under constant load point velocity were simulated using a spring-slider model obeying rate and state friction [*Dieterich*, 1978; *Ruina*, 1983]. We assume the following constitutive equation at the sliding interface,

$$\mu = \mu_o + a \ln\left(\frac{V}{V_o}\right) + b \ln\left(\frac{V_o \theta}{D_c}\right) \quad (1)$$

Table 1. List of Experiments[a]

Test #	Sample Type	Temperature, (°C)	Normal Stress (MPa)	Min V^*, (mm/s)	Max V^*, (mm/s)	H_2O Added	Style of Test	Extra (112 mm) Total Slip
d215-98	Solid	20	5	10^{-3}	10^{-3}	No	CLPV	No
d215-119	Solid	100	5	10^{-3}	10^{-3}	No	CLPV	No
d215-101	Solid	200	5	10^{-3}	10^{-3}	No	CLPV	No
d215-65	Solid	300	5	10^{-3}	10^{-3}	No	CLPV	No
d215-61	Solid	400	5	10^{-3}	10^{-3}	No	CLPV	No
d215-57	Solid	500	5	10^{-3}	10^{-3}	No	CLPV	No
d215-52	Solid	600	5	10^{-3}	10^{-3}	No	CLPV	No
d216-42	Gouge	20	5	3×10^{-4}	3×10^{-2}	No	VS	No
d216-51	Gouge	100	5	3×10^{-4}	3×10^{-2}	No	VS	No
d216-36	Gouge	200	5	3×10^{-4}	3×10^{-2}	No	VS	No
d216-52	Gouge	300	5	3×10^{-4}	3×10^{-2}	No	VS	No
d216-56	Gouge	400	5	3×10^{-4}	3×10^{-2}	No	VS	No
d216-71	Gouge	500	5	3×10^{-4}	3×10^{-2}	No	VS	No
d221-25	Gouge	600	5	10^{-3}	10^{-3}	No	CLPV	No
d216-43	Gouge	20	30	3×10^{-4}	3×10^{-2}	No	VS	No
d216-46	Gouge	100	30	3×10^{-4}	3×10^{-2}	No	VS	No
d216-32	Gouge	200	30	3×10^{-4}	3×10^{-2}	No	VS	No
d216-53	Gouge	300	30	3×10^{-4}	3×10^{-2}	No	VS	No
d216-59	Gouge	400	30	3×10^{-4}	3×10^{-2}	No	VS	No
d221-23	Gouge	500	30	10^{-3}	10^{-3}	No	CLPV	No
d221-24	Gouge	600	30	10^{-3}	10^{-3}	No	CLPV	No
d221-49	Gouge	300	30	10^{-3}	10^{-3}	No	CLPV	Yes
d221-37	Gouge	500	30	10^{-3}	10^{-3}	No	CLPV	Yes
d221-49	Gouge	300	30	10^{-3}	10^{-3}	Yes	CLPV	Yes
d221-37	Gouge	500	30	10^{-3}	10^{-3}	Yes	CLPV	Yes
d223-7,8	Gouge	500	30	10^{-5}	10^{-5}	No	CLPV	No
d223-8,9	Gouge	500	30	10^{-5}	10^{-5}	Yes	CLPV	No
d216-16	Gouge	20	5	0	10^{-2}	No	SHS	No
d216-50	Gouge	100	5	0	10^{-2}	No	SHS	No
d216-35	Gouge	200	5	0	10^{-2}	No	SHS	No
d216-55	Gouge	300	5	0	10^{-2}	No	SHS	No
d216-77	Gouge	400	5	0	10^{-2}	No	SHS	No
d216-75	Gouge	500	5	0	10^{-2}	No	SHS	No
d216-65	Gouge	600	5	0	10^{-2}	No	SHS	No
d216-44	Gouge	20	30	0	10^{-2}	No	SHS	No
d216-47	Gouge	100	30	0	10^{-2}	No	SHS	No
d216-33	Gouge	200	30	0	10^{-2}	No	SHS	No
d216-54	Gouge	300	30	0	10^{-2}	No	SHS	No
d216-60	Gouge	400	30	0	10^{-2}	No	SHS	No
d216-41	Gouge	500	30	0	10^{-2}	No	SHS	No
d216-64	Gouge	600	30	0	10^{-2}	No	SHS	No
d223-20	Gouge	500	40	10^{-3}	10^{-3}	No	CLPV	No
d223-20	Gouge	500	40	10^{-2}	10^{-2}	No	CLPV	No
d223-27	Gouge	500	30	10^{-3}	10^{-3}	No	CLPV	No

[a] Abbreviations for style of test: CLPV, constant load point velocity; VS, velocity stepping; SHS, slide-hold-slide.

where μ is the coefficient of friction, V is the slip velocity, μ_o is the coefficient of friction at reference velocity V_o, a is the direct velocity effect, b is the evolution effect, θ is the state variable, and D_c is the slip-weakening distance [*Dieterich*, 1979; *Ruina*, 1983].

Several expressions have been proposed to describe evolution of the state variable θ, including the aging law [*Dieterich*, 1979] and the slip law [*Ruina*, 1983],

$$\dot{\theta} = 1 - \frac{V\theta}{D_c}, \text{ Aging Law} \tag{2}$$

$$\dot{\theta} = -\frac{V\theta}{D_c} \ln\left(\frac{V\theta}{D_c}\right), \text{ Slip Law} \tag{3}$$

where the dot operator denotes differentiation with respect to time. At steady state ($\dot{\theta}$=0), equation (1) reduces to

$$\mu_{ss} = \mu_o + (a-b) \ln\left(\frac{V}{V_o}\right), \tag{4}$$

where μ_{ss} is the steady state friction at constant velocity V.

Consideration of evolution laws that are more complex compared to equations (2) and (3) [e.g., *Kato and Tullis*, 2001; *Nagata et al.*, 2012] did not result in improvements of model fit to the data [*Mitchell et al.*, 2015], and therefore here we present only results corresponding to the aging law and the slip law. The relationship between the stressing rate $\dot{\tau}$ and the rate of stretching of a thick metal bar (analog of a spring) that connects the stepper motor to the specimen holder follows from the Hooke's law and is given by

$$\dot{\tau} = k(V^* - V) \tag{5}$$

where k is the effective rigidity (spring constant) and V^* is the load point velocity. Equation (5) does not include an inertial term because the latter is negligible compared to the elastic stiffness term, as indicated by a dimensional analysis and confirmed by simulations that took into account inertial effects.

The coupled system of equations (2) and (7) and the respective evolution law was solved using Matlab's stiff ordinary differential equation solver "ode23s" subject to initial conditions of $[\delta_o, \tau_o, \theta_o]=[0, \mu_o\sigma, D_c/V_o]$, where δ is slip. The predicted shear stress time series was shifted in time to achieve the best agreement (using cross correlation) with the observed shear stress time series. The shift is necessary because the observed time series begins at an arbitrary point during the stick-slip cycle. The misfit between the two time series was then evaluated by computing the sum of the squares of the difference between the data and the model. This process was repeated for a range of values of the rate-state parameters $(a-b)$, $(a+b)$, D_c, and μ_o (and c in case of the modified aging law). The best fitting parameter values were chosen to be those that rendered the smallest misfit. This process was repeated for data from experiments conducted at different temperatures.

4. Results

We find that tests performed on bare surfaces show increasingly larger stick-slip events with temperature (Figure 2). Tests performed on simulated gouge samples show stable sliding at low temperatures. Velocity-stepping tests indicated velocity-strengthening behavior of gouge at low temperatures (Figures 3a, 3b, and 3d). However, at temperature above 200°C, the rate dependence of friction transitioned to velocity weakening (Figures 3a, 3c, and 3e and Figures S2 and S3 in the supporting information). To investigate the effect of total displacement, we repeated tests after accumulating more than 110 mm of total slip on the samples. We found that $(a-b)$ became slightly more negative, perhaps due to increased slip localization and further development of shear fabric.

Figure 4 shows a comparison of the data and the best fitting models (Figures 4a, 4b, 4d, and 4e) and an example of the misfit distribution as a function of parameters $(a-b)$ and $(a+b)$ for the aging law and the slip law (Figures 4c and 4f). We consistently find that the aging law provides a better fit to the data over a wide range of conditions compared to the slip law (Figures 4a, 4b and 4d, 4e). In particular, models assuming the slip law that are able to match the recurrence interval between slip events underpredict stress drops and slip rate during slip events (Figures 4d and 4e). Figure 5 shows the dependence of the best fitting rate and state parameters on temperature inferred from the models assuming the aging law. For velocity-stepping tests, rate and state parameters were measured directly from the data.

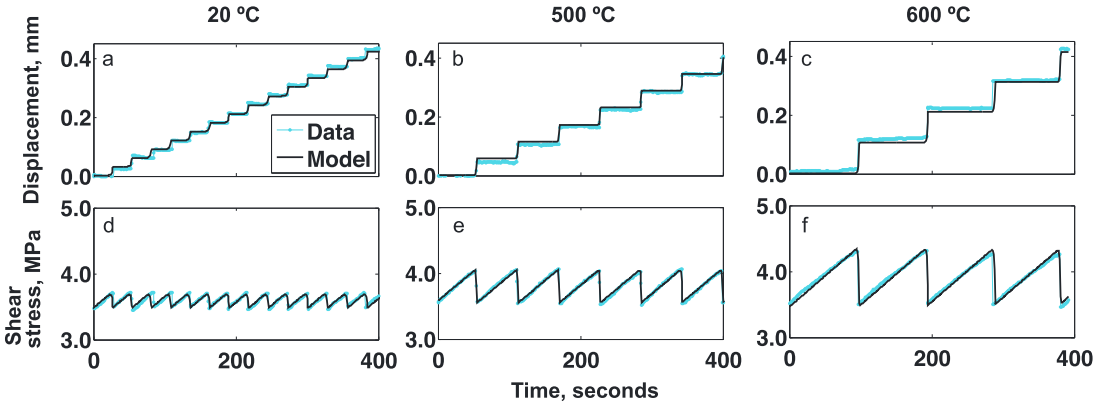

Figure 2. Stick-slip time series, solid sample of Westerly granite. Displacement time series at (a) 20, (b) 500, and (c) 600°C. The tests were conducted at 5 MPa normal stress and 10^{-3} mm/s load point velocity. Corresponding shear stress time series. Cyan dotted lines represent data, black lines represent predictions from the best fitting models. Subtracted linear trends T (MPa/s): (d) 1.5×10^{-6}; (e) 2.8×10^{-4}; (f) 3.4×10^{-4}. Data are from tests d215-52, d215-57, and d215-98 (see Table 1).

4.1. Microstructural Observations of a Shear Interface

To examine the structure of the slip interface, we extracted the gouge samples at the end of the tests. The samples were impregnated with epoxy and then cut into thin sections to observe shear microstructures. A thin-section analysis indicated that much of the gouge was consolidated except across a well-developed primary slip interface (Figures 1c and 1d). There is a pronounced grain size reduction toward the primary slip interface, where the maximum grain size is on the order of 10^{-4} m and most of the grains have dimensions on the order of microns or less (Figure 1b). The dramatic grain size reduction toward the slip zone can be seen even without a microscope by viewing the sample from the side (Figure 1d, brownish upper half of the sample). Also conspicuous both on macro and micro scale are Riedel shears extending away from the primary

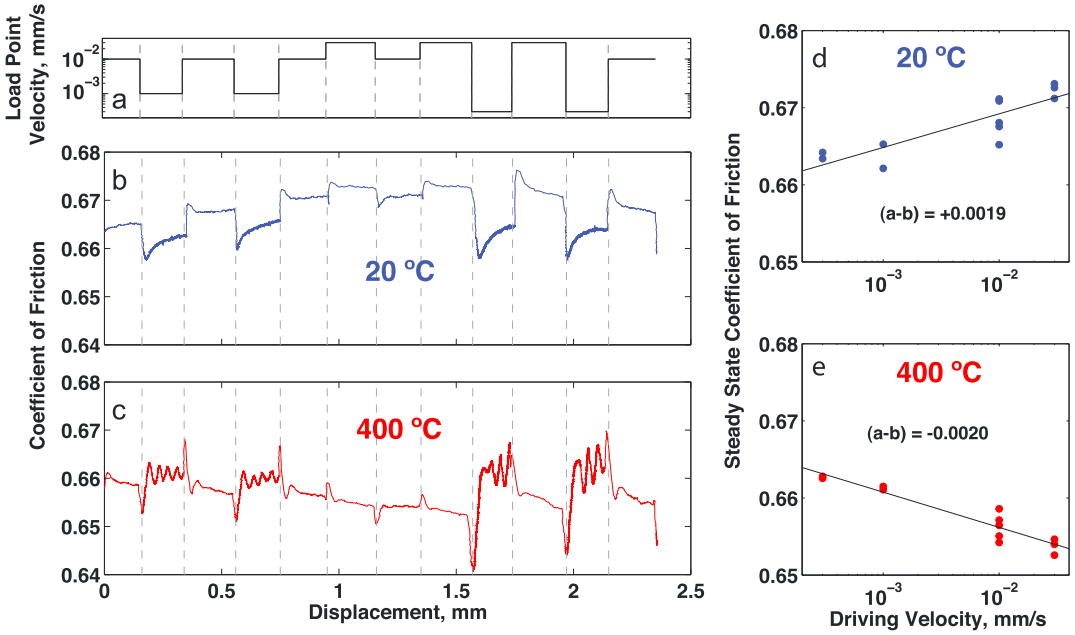

Figure 3. Results of velocity-stepping tests, Westerly granite gouge. (a) Load point velocity versus displacement. Coefficient of friction versus displacement at (b) 20°C (test d216-43) and (c) 400°C (test d216-59). Steady state coefficient of friction as a function of load point velocity at (d) 20°C (test d216-43) and (e) 400°C (test d216-59). Lines denote the least squares fit to the data. $(a - b)$ is the slope of the line. Tests were performed at a normal stress of 30 MPa. Subtracted linear trends T (mm^{-1}): 5.3×10^{-3} (Figure 3b); 2.1×10^{-3} (Figure 3c).

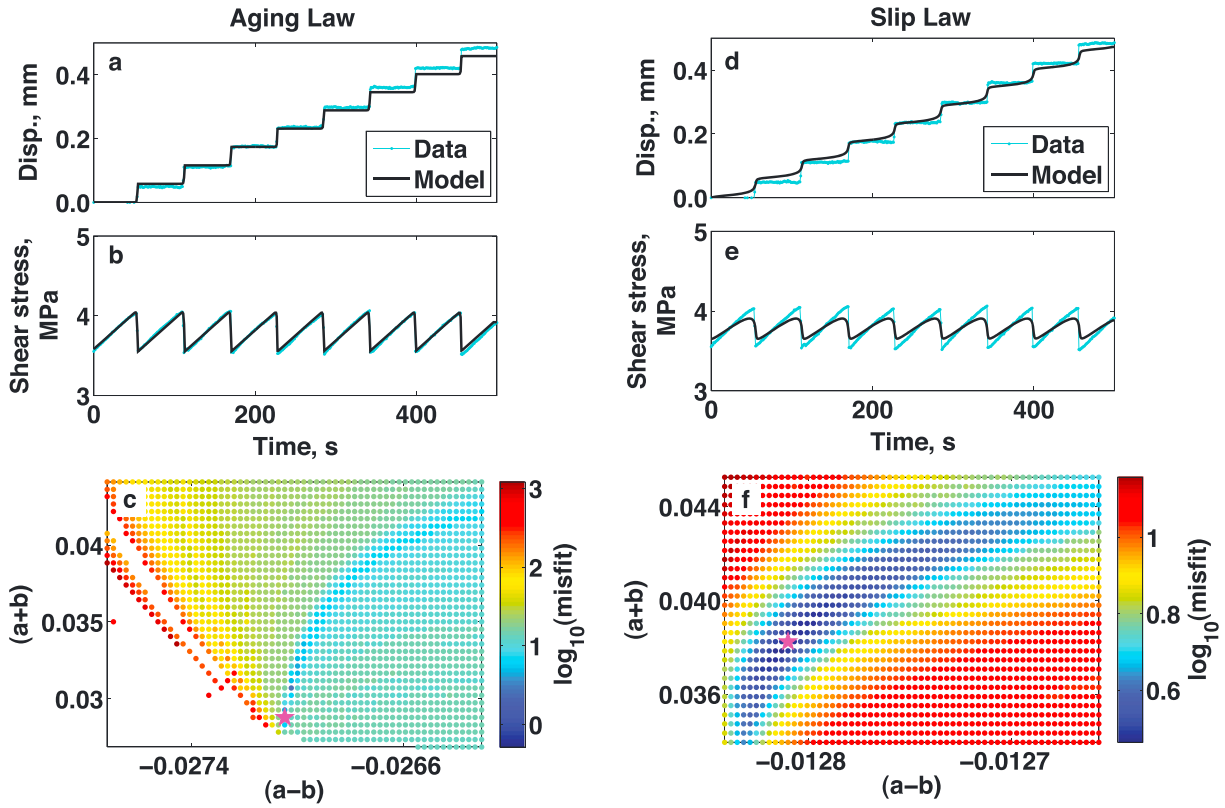

Figure 4. Observed (test d215-57) and modeled time series of displacement and shear stress assuming different evolution laws. In Figures 4a, 4b, 4d, and 4e, observations are denoted by cyan dots, and model predictions are denoted by black dots. Experiments were performed on solid samples of Westerly granite at temperature of 500°C, normal stress of 5 MPa, and load point velocity of 10^{-3} mm/s. (a, d) Displacements. (b, e) Shear stress. Linear trend subtracted from the data $T = 2.8 \times 10^{-4}$ MPa s^{-1}. (c, f) Misfit between data and modeled shear stress as a function of the parameters $(a - b)$ and $(a + b)$ at the best fitting values for D_c and μ_o. Cool colors represent low misfit and warm colors represent high misfit. The magenta star marks the minimum misfit. Figures 5d and 5e show the same data set in light blue as in Figures 5a and 5b.

slip interface (e.g., Figure 1d). We observe sheared grains of biotite and cracked grains of feldspar that resemble deformed grains in granite from previous studies [e.g., *Stesky*, 1978]. Shear fabrics produced in our experiments (Figures 1b–1d) appear to share many similarities with those found on natural faults [e.g., *Chester and Logan*, 1987].

4.2. Effects of Loading Conditions

Tests done at different values of normal stress and load point velocities did not show any significant change in rate dependence of friction and the inferred value of $(a-b)$ at temperatures below 400°C. Provided that $(a-b)$ is negative and the machine stiffness k is below the limit of conditional stability $\sigma_n(b - a)/D_c$ [*Ruina*, 1983], where σ_n is the effective normal stress, the amplitude and the recurrence interval of stick slip is expected to progressively increase with increasing normal stress, as predicted by rate and state friction theory [e.g., *Heslot et al.*, 1994] and observed in our experiments (Figure S4).

To test the dependence of slip pattern on the load point velocity, we conducted a series of tests at velocity of 10^{-5} mm/s which is at the lower end of the range of load point velocities used in triaxial tests [*Lockner et al.*, 1986; *Blanpied et al.*, 1991] and more comparable to the loading rates of natural faults (centimeters per year, or $\sim 10^{-6}$ mm/s). We found that the lower load point velocity results in larger stress drop events with greater recurrence intervals (Figure 6). This is again consistent with predictions of the rate and state friction theory, as the contacting surfaces have more time to "heal" between slip events, thereby resulting in greater static friction and larger stress drops [e.g., *Gu et al.*, 1984; *Baumberger and Caroli*, 2006].

4.3. Effects of Water

The presence of water has a marked effect on frictional properties of gouge. At the beginning of injection, the samples sometimes begin to creep, but shortly thereafter, stick slip resumes, with larger amplitude and

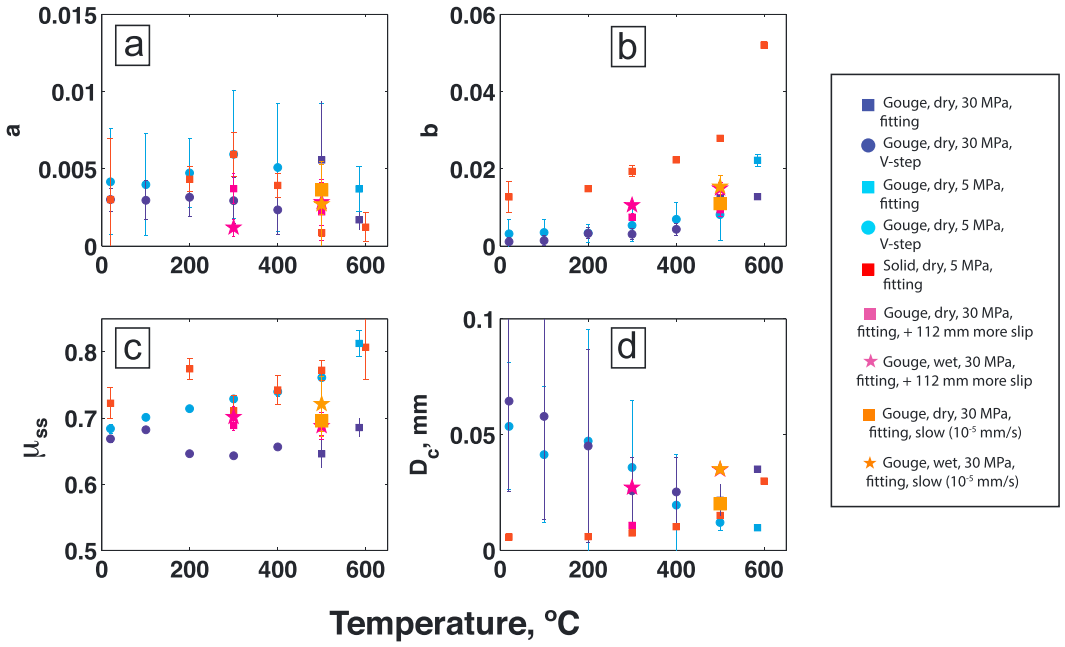

Figure 5. Rate and state parameters as a function of temperature. (a) The "direct effect," *a*. (b) The "evolution effect," *b*. (c) μ_{ss} at 10^{-2} mm/s. In case of unstable slip, μ_{ss} was calculated using equation (4) for $V = 10^{-2}$ mm/s. (d) Slip-weakening distance D_c. For Figures 5a–5d the error bars on velocity-stepping measurements (circles) represent 2 standard deviations. The error bars on parameter-fitting calculations (squares) represent the range in the parameter that produces triple the minimum misfit. Pink squares represent tests on Westerly granite gouge conducted at normal stress of 30 MPa and 112 mm more total slip compared to tests shown in dark blue. The orange square represents a test on Westerly granite gouge conducted at normal stress of 30 MPa and load point velocity of 10^{-5} mm/s. All other unsteady tests shown here were conducted at load point velocity of 10^{-3} mm/s. Stars denote parameters inferred (via model fitting) from tests under hydrated conditions. Data are from tests d215-52,57,61,65,98,101, d221-23,24,37,49, d216-32,42,43,46,51,53,56,59,71, and d223-7,8,9.

longer recurrence intervals compared to the dry tests (Figure 6), indicative of more negative $(a - b)$. After the water injection was stopped, the size of stick slips returned to smaller values similar to those before water was added.

Figure 7 shows a summary of $(a - b)$ values inferred from our experiments on solid and gouge samples under dry and hydrated conditions as a function of temperature (solid colored symbols), as well as results from previous triaxial tests (open black symbols). Our results for dry gouge are in general agreement with those from previous studies [*Lockner et al.*, 1986] (Figure 7, solid circles versus open circles) up to a temperature of about 350°C. Above 350°C, there is a general disagreement between different sets of experiments. *Stesky* [1978] reported increasing values of $(a - b)$ with temperature, while *Lockner et al.* [1986] found $(a - b)$ to be slightly positive and independent of temperature. Our data for dry gouge indicate that $(a - b)$ continues to become increasingly negative at temperatures above 350°C. This behavior is even more pronounced in tests on solid samples (see red squares in Figure 7). The effects of water on the rate dependence of friction appear to enhance the high-temperature trends observed in different experiments under dry conditions. Triaxial tests conducted at confined hydrothermal conditions show more negative values of $(a - b)$ compared to dry tests at temperatures between 100 and 350°C (Figure 7, open triangles versus open circles). Our experiments conducted at dry and hydrated conditions show a similar behavior over the respective temperature range (Figure 7, pink squares versus pink stars). However, at temperatures above 350°C the data are remarkably different. Triaxial tests of *Blanpied et al.* [1991] showed that in the presence of water, friction becomes more velocity strengthening, i.e., $(a - b)$ is positive and increasing with temperature, while our direct shear tests indicate that $(a - b)$ is negative and continues to decrease over the entire temperature range up to 600°C (Figure 7, filled symbols).

Modeling of stress histories associated with unstable slip using rate and state friction theory reveals that the observed decrease in $(a - b)$ with temperature occurs primarily due to an increase in the "evolution" parameter *b* (Figures 5b and S1d). The parameter *b* characterizes the rate of healing of a slip interface, often attributed to a

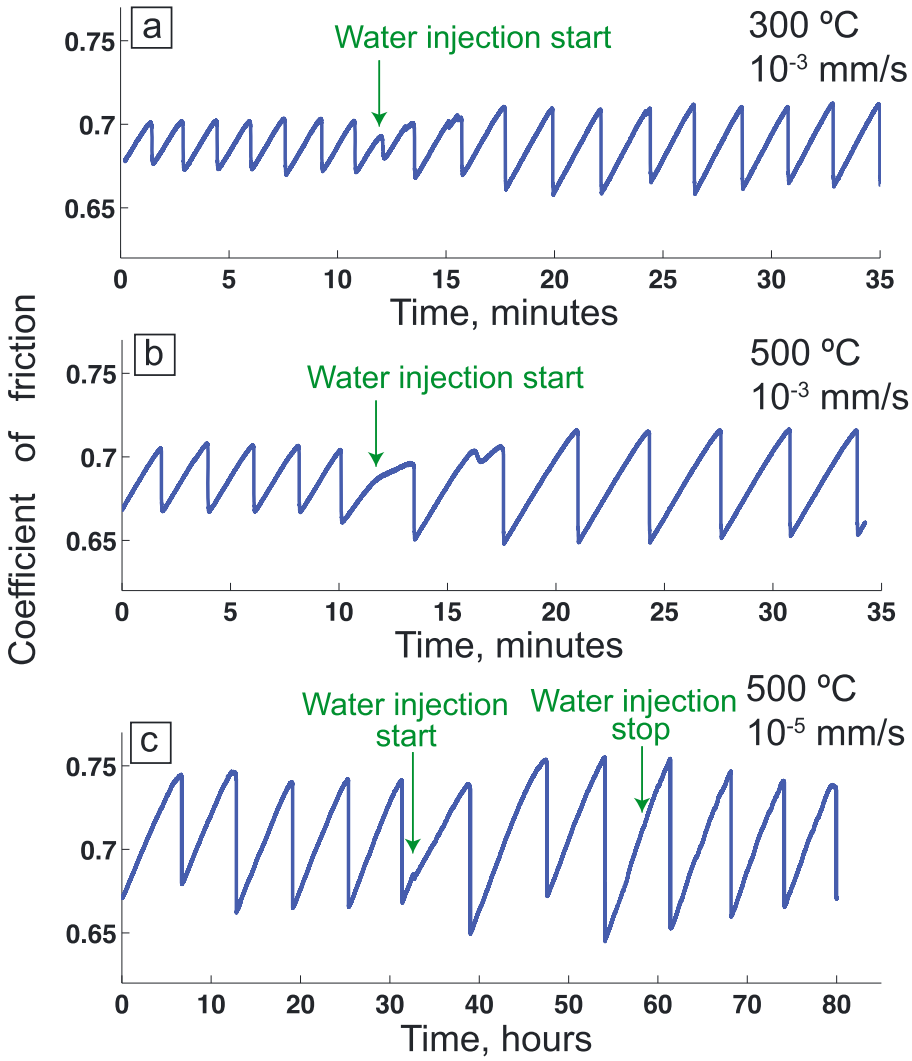

Figure 6. Dry versus hydrated Westerly granite gouge. (a) Coefficient of friction from a test conducted at temperature of 300°C, normal stress of 30 MPa, and load point velocity of 10^{-3} mm/s. Water was injected into the bottom of the sample at a rate of 2 mL/min starting at the time indicated by the green arrow and continuing through the rest of the test (test d221-49). $T = 1.6 \times 10^{-5}$ s^{-1}. (b) Same as Figure 6a, at temperature of 500°C (test d221-37). $T = 5.3 \times 10^{-6}$ s^{-1}. (c) Same as Figure 6b, at load point velocity of 10^{-5} mm/s (tests d223-7,8,9,10). $T = 1.6 \times 10^{-7}$ s^{-1}. Water was injected for the time period marked by the two green arrows. In all tests the maximum injection pressure (and thus pore pressure) was limited to 0.7 MPa (100 psi).

time-dependent increase in real contact area due to creep at microscopic asperities [*Dieterich*, 1972; *Dieterich and Kilgore*, 1994]. Higher temperatures are expected to enhance frictional healing, resulting in greater values of *b* [*Nakatani*, 2001; *Mitchell et al.*, 2013]. While the parameter *a* is also expected to increase with temperature [e.g., *Nakatani*, 2001; *Rice et al.*, 2001], the observed tendency for more unstable slip at greater temperature in our experiments (Figures 2, S2, and S3) indicates that the parameter *b* is increasing with temperature at a greater rate than the parameter *a*. Due to trade-offs between model parameters in numerical simulations of unstable slip, the difference $(a-b)$ is better constrained than parameters *a* and *b* individually. Because of large uncertainties in the estimates of parameter *a*, no systematic dependence of *a* on temperature can be seen in our best fit models (Figure 5a).

5. Discussion

The dependence of frictional properties on a type of an experimental apparatus at high temperatures (Figure 7) is surprising, as the experiments were conducted on the same rock type and over a similar range of

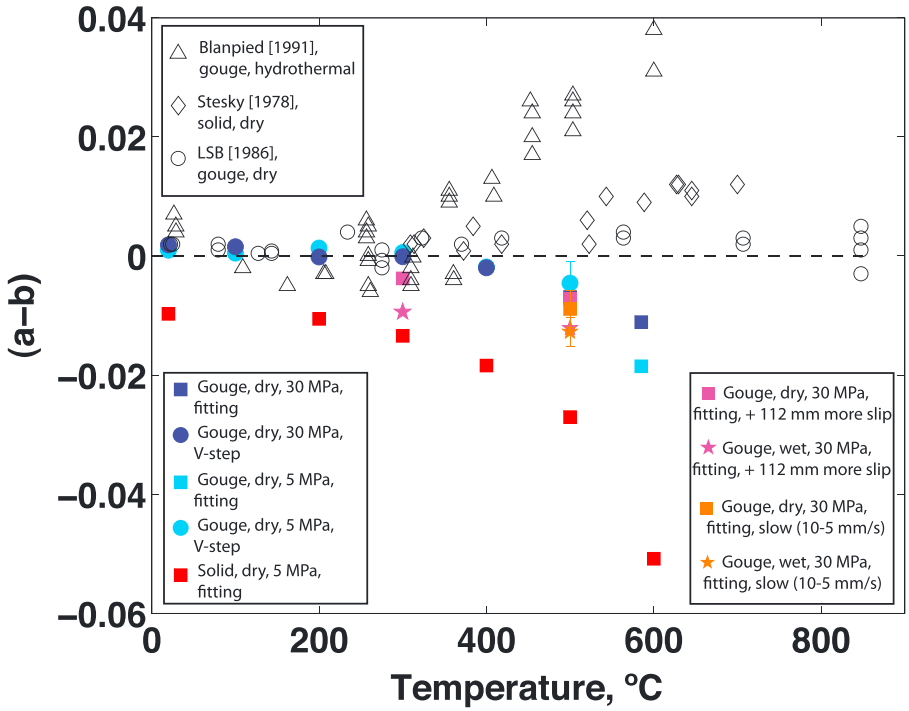

Figure 7. The $(a - b)$ versus temperature, Westerly granite. Open symbols denote results from previous studies. Filled symbols denote results from this study. Error bars on symbols representing velocity-stepping tests correspond to 2 standard deviations. Error bars on symbols representing model fits to the time series correspond to the variation in $(a - b)$ that triples the minimum misfit at a given temperature. Same test numbers as in Figure 5.

temperatures and slip rates. The main differences are the total slip, normal stress, and pore pressure. While the direct shear apparatus allows for a much larger total slip (thus yielding a greater similarity to natural faults), we do not believe that this fully explains the observed difference, as direct shear experiments with even a limited amount of slip exhibited velocity-weakening properties similar to those shown in Figure 7, albeit of a smaller magnitude.

5.1. Effects of Normal Stress and Pore Pressure

The triaxial experiments were conducted at greater normal stresses and pore pressures (of the order of hundreds of megapascals), compared to the direct shear experiments. One could argue that the presence of water may help stabilize slip at high temperature by enhancing creep rate at the scale of microasperities [*Blanpied et al.*, 1995]. Temperature and water content are expected to have similar effects on friction, as both factors contribute to lowering the effective viscosity of the asperity contacts. However, the overall impact on frictional strength (and rate dependence of friction) is not straightforward. There is a competition between a possible reduction in shear strength of the asperities and an increase in the asperity size (and the true area of contact) [*Mitchell et al.*, 2013]. Other processes such as hydrogen bonding, desorption of water, and water-aided crack growth may contribute to more efficient frictional healing under hydrated conditions [*Dieterich and Conrad*, 1984; *Frye and Marone*, 2002]. High pore pressures may be an important factor promoting stable creep at high temperature due to, e.g., increased water fugacity and various hydrolytic reactions [*Blanpied et al.*, 1995; *den Hartog et al.*, 2014]. If the magnitude of pore pressure is the main reason for the differences between the high-temperature results from the triaxial and direct shear apparati, our observations suggest that the effect of pore pressure on the rate dependence of friction is highly nonlinear, with low pore pressure enhancing velocity-weakening, and high pore pressure enhancing velocity-strengthening behavior (Figure 7). This suggests an intriguing possibility that unsteady slip below the nominal brittle-ductile transition (e.g., microearthquakes, low-frequency earthquakes, and tremor) might result from spatial variations in water content and/or pore fluid pressure in the middle and lower crust. In this case, locally dry or underpressurized regions may act as nucleation sites of slip instabilities. Subsequent evolution and magnitude of slip instabilities will depend on how the characteristic dimensions of low pore pressure regions D compare to the nucleation length scale $L = D_c G/[(1 - \nu)b\sigma_n]$, where G is the shear modulus, and ν is the Poisson ratio

[e.g., *Dieterich*, 1992; *Fialko*, 2015]. Slow slip and tremor may occur when $D < L$. Regular earthquakes may occur when $D/L \gg 1$ (with D providing an upper limit on the earthquake magnitude unless strong dynamic weakening is activated). It should be noted, however, that at temperature and pressure conditions corresponding to the lower crust, porosities are small and water is likely to be absorbed into hydrous mineral phases, so that little, if any, water may exist in a free fluid phase [*Newton*, 1990]. We also note that a disagreement between the triaxial and direct shear experiments for temperatures greater than 350°C under dry conditions (Figure 7) cannot be attributed to the effects of pore pressure.

Increases in normal stress (or, in the presence of pore fluids, the effective normal stress) alone are not expected to promote stable slip provided that the ratio of a true contact area to the total surface area remains sufficiently small [*Dieterich and Kilgore*, 1994; *Mitchell et al.*, 2013]. However, there is some experimental evidence that the rate-weakening parameter $(a-b)$ may depend on normal stress [e.g., *Saffer and Marone*, 2003; *Ikari et al.*, 2009; *Niemeijer and Vissers*, 2014; *den Hartog et al.*, 2014; *Sawai et al.*, 2016]. In particular, *Niemeijer and Vissers* [2014] reported an increase in $(a - b)$ with normal stress for phyllosilicate-rich gouges from the Alhama de Murcia Fault in southeast Spain. At the same time, no systematic dependence of $(a - b)$ on normal stress was found for more competent phyllitic protolyth from the same location [*Niemeijer and Vissers*, 2014]. *Sawai et al.* [2016] found no dependence of $(a - b)$ of blueschist gouge on normal stress at temperature up to 200°C and a systematic increase in $(a - b)$ with normal stress at higher temperature. Our experiments also do not reveal any dependence of $(a-b)$ parameter on normal stress for Westerly granite gouge at low-to-intermediate temperature. At temperature above 300°C, there is an indication of a less negative value of $(a - b)$ at higher normal stress (see light and dark blue square symbols in Figure 7). Extrapolation of this trend to higher normal stresses predicts a transition to velocity-strengthening behavior for $\sigma_n > 10^2$ MPa, which might possibly reconcile our results with those obtained on triaxial machines (although note that velocity-weakening behavior was in fact observed in some of the triaxial experiments of *Lockner et al.* [1986] at the high end of the tested temperature range, see Figure 7). This would imply that the effect of increasing normal stress on the rate dependence of friction is opposite to that of temperature, and the two effects compete with each other as both pressure and temperature increase with depth. If so, experimental studies of the depth dependence of $(a - b)$ need to vary both normal stress and temperature to adequately approximate in situ conditions; inferences based on a single variable (either normal stress or temperature) as a proxy for depth should be treated with caution. These conclusions can be tested by performing experiments in the intermediate range of normal stresses (50–300 MPa) at high temperatures (>400°).

5.2. Implications for the Depth of the Seismic-Aseismic Transition

Results presented in this study further indicate that the rate dependence of friction of typical crystalline rocks such as granite and the depth extent of seismicity in continental crust cannot be simply attributed to thermally activated onset of plasticity in either quartz (at ~300°) or plagioclase (at ~450°), as commonly assumed [e.g., *Scholz*, 2002, p. 152]. Other factors that may affect the depth distribution of earthquakes include compositional changes (e.g., a decrease in silica content with depth), variations in water content, and delocalization of slip below the brittle-ductile transition [*Chen and Molnar*, 1983; *Leloup et al.*, 1995; *Wilson et al.*, 2004; *Takeuchi and Fialko*, 2012]. Recent high-temperature triaxial tests on gabbroic gouge indicated velocity-weakening behavior up to 600°C [*He et al.*, 2013]. Direct shear experiments on gabbro at conditions analogous to those in this study also show a progressive decrease in the rate parameter $(a - b)$ with temperature, with a transition to velocity weakening above 150°C for bare surfaces, and 300°C for thick gouges [*Mitchell et al.*, 2015]. These findings, along with results presented in this study, imply that the middle and lower continental crust can be seismically active under certain conditions. Deep crustal seismicity in fact appears to be quite common in a variety of tectonic settings including areas of active extension (e.g., Baikal [*Emmerson et al.*, 2006] and East Africa [*Craig et al.*, 2011] rift zones) and convergence (e.g., Himalayas [*Jackson*, 2002] and Andes [*Leyton et al.*, 2009]). In other areas where the lower crust is predominantly aseismic, sparse microseismicity and nonvolcanic tremor [e.g., *Shelly*, 2010; *Trugman et al.*, 2015; *Inbal et al.*, 2015] indicate that conditions for unstable slip can be met locally, while the bulk of the crust is velocity strengthening. In case the rate-weakening effect of hydrous fluids at low pore pressure observed in our experiments (Figures 6 and 7) persists at high normal stresses, the observed variations in the depth distribution of seismicity could result from regional and local variations in water content and/or pore pressure, as discussed above. Given the importance of laboratory data for our understanding of the occurrence and distribution of earthquakes in seismically active areas, the effects of normal stress and pore pressure on slip stability need to be better constrained over the representative range of temperatures.

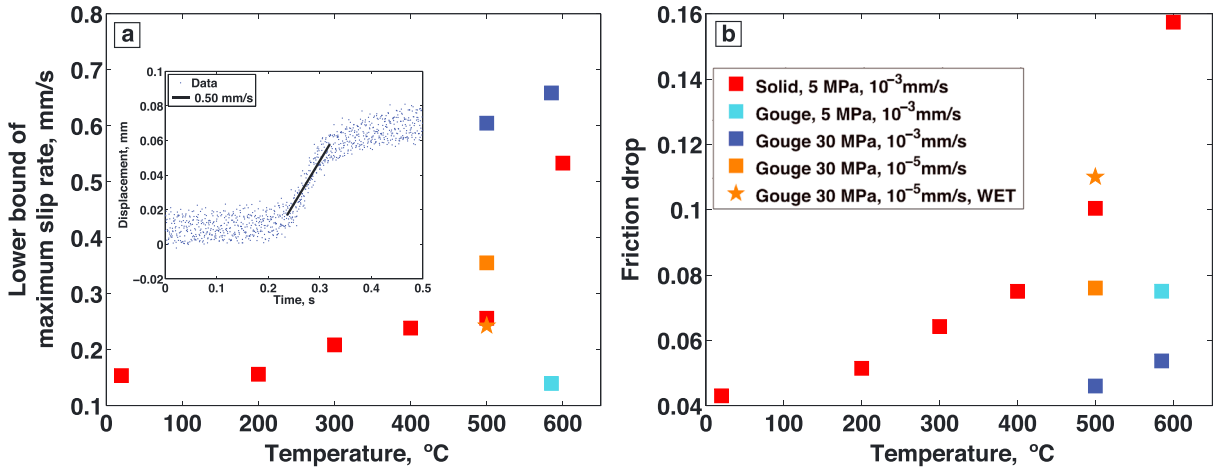

Figure 8. Maximum slip rate and drop in coefficient of friction for stick-slip events: (a) Maximum slip rate during slip events versus temperature. For most tests, data were collected at a rate of 10 samples/s, and represent a lower bound on the maximum slip rate during slip events. The inset figure shows the displacement time series for a slip event sampled at a higher rate (1987 samples/s, blue dots; test d223-27). The slope of the black line, which represents the maximum slip rate during the slip event, is 0.5 mm/s. Symbols are the same as those in Figure 7. (b) Drop in coefficient of friction during slip events versus temperature. Symbols are the same as those in Figure 7. Same test numbers as in Figure 5.

The enhanced velocity weakening due to decreases in the $(a - b)$ parameter observed in our experiments (Figure 7) can be also relevant to the dynamics of earthquake ruptures, as frictional heating during rapid coseismic slip may substantially perturb temperature on a slip interface [e.g., *Jeffreys*, 1942; *McKenzie and Brune*, 1972; *Fialko*, 2004]. A number of dynamic mechanisms have been proposed to affect shear strength of rocks at seismic slip rates (order of 1 m/s), based on theoretical arguments and experimental observations [e.g., *Sibson*, 1973; *Tsutsumi and Shimamoto*, 1997; *Di Toro et al.*, 2004; *Fialko and Khazan*, 2005; *Rice*, 2006; *Han et al.*, 2007; *Goldsby and Tullis*, 2011; *Brown and Fialko*, 2012]. We note that the enhanced velocity weakening observed in our experiments at high temperature unlikely results from dynamic mechanisms, as the measured sample velocities during slip events are less than 1 mm/s (Figure 8), well below slip rates associated with dynamic weakening in high-speed friction experiments [e.g., *Reches and Lockner*, 2010, *Reches and Lockner*, 2010; *Di Toro et al.*, 2011; *Brown and Fialko*, 2012]. The effect of temperature on fault strength is not straightforward, as decreases in $(a - b)$ with temperature may be counteracted by increases in μ_0; both triaxial and direct shear tests indicate that static friction increases with temperature, at least under dry conditions (Figure S1e) [*Stesky*, 1978; *Mitchell et al.*, 2013]. This strengthening is likely caused by increases in the quantity

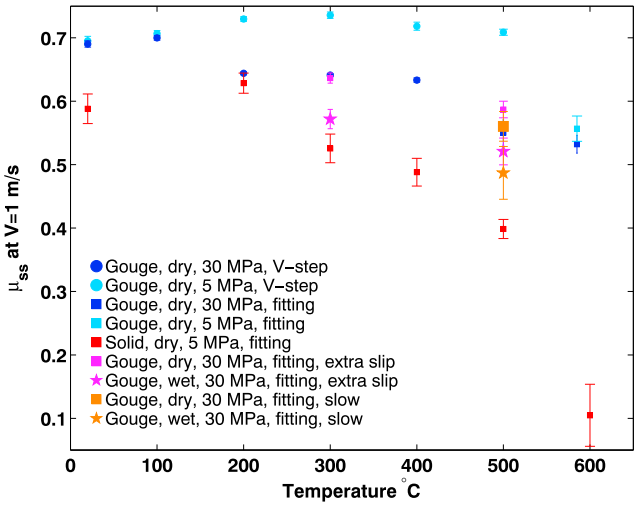

Figure 9. Steady state coefficient of friction μ_{ss} extrapolated to slip rate of 1 m/s. The μ_{ss} was computed using equation (4) and rate and state parameters shown in Figure 5. Enhanced velocity weakening dominates over increases in static friction at elevated temperature (>400°C, in particular, for bare surfaces. Same test numbers as in Figure 5.

and/or quality of contacts due to thermally activated creep at the asperity tips [*Mitchell et al.*, 2013]. At low slip rates, increases in friction with temperature indeed appear to dominate (Figure 5c). Extrapolation of our experimental data to seismic slip rates assuming the rate and state model (equation (4)) reveals a moderate reduction in shear strength for simulated gouges, and a significant reduction in shear strength for bare surfaces at ambient temperature >400°C (Figure 9). In the latter case, predicted weakening due to temperature dependence of $(a - b)$ is comparable in magnitude to dynamic weakening observed in high-speed rock friction experiments [*Tsutsumi and Shimamoto*, 1997; *Han et al.*, 2007; *Reches and Lockner*, 2010; *Di Toro et al.*, 2011; *Brown and Fialko*, 2012]. It is interesting to note that the dynamic weakening of crystalline rocks is usually much more pronounced in laboratory tests done on "bare surfaces" and/or in the presence of only a thin layer of gouge, compared to experiments done on thick gouge samples [e.g., *Proctor et al.*, 2014]. Results shown in Figure 9 offer an intriguing possibility that at least some dynamic weakening observed at high slip rates might be explained in the framework of rate and state friction provided that the temperature dependence of material parameters such as $(a - b)$ is properly taken into account.

6. Conclusions

Direct shear experiments on Westerly granite performed over a wide range of conditions including temperatures between 20 and 600°C, load point velocities 10^{-5} to 3×10^{-2} mm/s, normal stresses 5–40 MPa, on bare surfaces and simulated gouge, and on dry samples and in the presence of water reveal increasingly unstable slip behavior (enhanced velocity weakening) with temperature over the entire tested range of temperatures. Tests performed on solid samples reveal stronger velocity weakening compared to tests performed on simulated gouge. Enhanced velocity weakening was also observed under hydrated conditions (in the presence of water steam), compared to dry tests. The observed temperature dependence of the rate parameter $(a - b)$ is substantially different from that reported in high-temperature triaxial experiments performed at higher normal stresses and pore pressures. This difference may be due to a strong dependence of $(a - b)$ on normal stress and/or pore pressure at temperatures greater than ~400°C. Results presented in this study suggest that the depth extent of the seismogenic zone in continental crust may not be fully controlled by the onset of plasticity in either quartz or plagioclase, and that frictional properties of common crustal rocks can be velocity weakening over a wider depth range than previously believed, in particular, under dry conditions or low pore pressure.

Acknowledgments
This work was supported by NSF (grants EAR-0838255 and 1321932). We thank three anonymous reviewers and the Associate Editor for their detailed comments that improved the manuscript. Data and modeling results presented in this study are available from the authors.

References

Baumberger, T., and C. Caroli (2006), Solid friction from stick-slip down to pinning and aging, *Adv. Phys.*, *55*(3–4), 279–348, doi:10.1080/00018730600732186.
Beeler, N. M., T. E. Tullis, and J. D. Weeks (1994), The roles of time and displacement in the evolution effect in rock friction, *Geophys. Res. Lett.*, *21*(18), 1987–1990, doi:10.1029/94GL01599.
Blanpied, M. L., D. A. Lockner, and J. D. Byerlee (1991), Fault stability inferred from granite sliding experiments at hydrothermal conditions, *Geophys. Res. Lett.*, *18*(4), 609–612.
Blanpied, M. L., D. A. Lockner, and J. D. Byerlee (1995), Frictional slip of granite at hydrothermal conditions, *J. Geophys. Res.*, *100*(B7), 13,045–13,064.
Brace, W., and J. Byerlee (1966), Stick-slip as a mechanism for earthquakes, *Science*, *153*(3739), 990–992.
Brown, K. M., and Y. Fialko (2012), "Melt welt" mechanism of extreme weakening of gabbro at seismic slip rates, *Nature*, *488*(7413), 638–641.
Chen, W.-P., and P. Molnar (1983), Focal depths of intracontinental and intraplate earthquakes and their implications for the thermal and mechanical properties of the lithosphere, *J. Geophys. Res.*, *88*(B5), 4183–4214.
Chester, F., and J. Logan (1987), Composite planar fabric of gouge from the punchbowl fault, California, *J. Struct. Geol.*, *9*(5), 621–634.
Craig, T., J. Jackson, K. Priestley, and D. McKenzie (2011), Earthquake distribution patterns in Africa: Their relationship to variations in lithospheric and geological structure, and their rheological implications, *Geophys. J. Int.*, *185*(1), 403–434.
den Hartog, S. A., D. M. Saffer, and C. J. Spiers (2014), The roles of quartz and water in controlling unstable slip in phyllosilicate-rich megathrust fault gouges, *Earth Planets Space*, *66*(1), 78.
Di Toro, G., D. L. Goldsby, and T. E. Tullis (2004), Friction falls towards zero in quartz rock as slip velocity approaches seismic rates, *Nature*, *427*(6973), 436–439.
Di Toro, G., R. Han, T. Hirose, N. De Paola, S. Nielsen, K. Mizoguchi, F. Ferri, M. Cocco, and T. Shimamoto (2011), Fault lubrication during earthquakes, *Nature*, *471*(7339), 494–498.
Dieterich, J. H. (1972), Time-dependent friction in rocks, *J. Geophys. Res.*, *77*(20), 3690–3697, doi:10.1029/JB077i020p03690.
Dieterich, J. H. (1974), Earthquake mechanisms and modeling, *Annu. Rev. Earth Planet. Sci.*, *2*, 275–301.
Dieterich, J. H. (1978), Time-dependent friction and the mechanics of stick-slip, *Pure Appl. Geophys.*, *116*, 790–806, doi:10.1007/BF00876539.
Dieterich, J. H. (1979), Modeling of rock friction 1. Experimental results and constitutive equations, *J. Geophys. Res.*, *84*(B5), 2161–2168, doi:10.1029/JB084iB05p02161.
Dieterich, J. H. (1992), Earthquake nucleation on faults with rate- and state-dependent strength, *Tectonophysics*, *211*, 115–134.
Dieterich, J. H., and G. Conrad (1984), Effect of humidity on time- and velocity-dependent friction in rocks, *J. Geophys. Res.*, *89*(B6), 4196–4202, doi:10.1029/JB089iB06p04196.

Dieterich, J. H., and B. D. Kilgore (1994), Direct observation of frictional contacts: New insights for state-dependent properties, *Pure Appl. Geophys.*, *143*, 283–302, doi:10.1007/BF00874332.
Eaton, J., M. O'neill, and J. Murdock (1970), Aftershocks of the 1966 Parkfield-Cholame, California, earthquake: A detailed study, *Bull. Seismol. Soc. Am.*, *60*(4), 1151–1197.
Emmerson, B., J. Jackson, D. McKenzie, and K. Priestley (2006), Seismicity, structure and rheology of the lithosphere in the Lake Baikal region, *Geophys. J. Int.*, *167*(3), 1233–1272.
Fialko, Y. (2004), Temperature fields generated by the elastodynamic propagation of shear cracks in the Earth, *J. Geophys. Res.*, *109*, B01303, doi:10.1029/2003JB002497.
Fialko, Y. (2015), Fracture and frictional mechanics—Theory, in *Treatise on Geophysics*, vol. 4, 2nd ed., edited by G. Schubert, pp. 73–91, Elsevier, Oxford, U. K.
Fialko, Y., and Y. Khazan (2005), Fusion by earthquake fault friction: Stick or slip?, *J. Geophys. Res.*, *110*, B12407, doi:10.1029/2005JB003869.
Franck, E. (1983), Thermophysical properties of supercritical fluids with special consideration of aqueous systems, *Fluid Phase Equilib.*, *10*(2), 211–222.
Frye, K. M., and C. Marone (2002), Effect of humidity on granular friction at room temperature, *J. Geophys. Res.*, *107*(B11), 2309, doi:10.1029/2001JB000654.
Goldsby, D. L., and T. E. Tullis (2011), Flash heating leads to low frictional strength of crustal rocks at earthquake slip rates, *Science*, *334*(6053), 216–218.
Gu, J.-C., J. R. Rice, A. L. Ruina, and S. T. Tse (1984), Slip motion and stability of a single degree of freedom elastic system with rate and state dependent friction, *J. Mech. Phys. Solids*, *32*, 167–196.
Han, R., T. Shimamoto, T. Hirose, J.-H. Ree, and J. Ando (2007), Ultralow friction of carbonate faults caused by thermal decomposition, *Science*, *316*, 878–881.
He, C., L. Luo, Q.-M. Hao, and Y. Zhou (2013), Velocity-weakening behavior of plagioclase and pyroxene gouges and stabilizing effect of small amounts of quartz under hydrothermal conditions, *J. Geophys. Res. Solid Earth*, *118*, 3408–3430, doi:10.1002/jgrb.50280.
Heslot, F., T. Baumberger, B. Perrin, and C. Caroli (1994), Creep, stick-slip, and dry-friction dynamics: Experiments and a heuristic model, *Phys. Rev. E*, *49*(6), 4973–4988.
Hill, D. P., P. Mowinckel, and L. G. Peake (1975), Earthquakes, active faults, and geothermal areas in the Imperial Valley, California, *Science*, *188*(4195), 1306–1308.
Ikari, M. J., D. M. Saffer, and C. Marone (2009), Frictional and hydrologic properties of clay-rich fault gouge, *J. Geophys. Res.*, *114*, B05409, doi:10.1029/2008JB006089.
Inbal, A., R. W. Clayton, and J.-P. Ampuero (2015), Imaging widespread seismicity at midlower crustal depths beneath Long Beach, CA, with a dense seismic array: Evidence for a depth-dependent earthquake size distribution, *Geophys. Res. Lett.*, *42*, 6314–6323, doi:10.1002/2015GL064942.
Jackson, J. (2002), Strength of the continental lithosphere: Time to abandon the jelly sandwich?, *GSA Today*, *12*(9), 4–9.
Jeffreys, H. (1942), On the mechanics of faulting, *Geol. Mag.*, *79*, 291–295.
Kato, N., and T. E. Tullis (2001), A composite rate-and state-dependent law for rock friction, *Geophys. Res. Lett.*, *28*(6), 1103–1106.
Leloup, P. H., R. Lacassin, P. Tapponnier, U. Schärer, D. Zhong, X. Liu, L. Zhang, S. Ji, and P. T. Trinh (1995), The Ailao Shan-Red River shear zone (Yunnan, China), Tertiary transform boundary of Indochina, *Tectonophysics*, *251*(1), 3–84.
Leyton, F., A. Pérez, J. Campos, R. Rauld, and E. Kausel (2009), Anomalous seismicity in the lower crust of the Santiago Basin, Chile, *Phys. Earth Planet. Inter.*, *175*(1), 17–25.
Lockner, D. A., R. Summers, and J. D. Byerlee (1986), Effects of temperature and sliding rate on frictional strength of granite, *Pure Appl. Geophys.*, *124*, 445–469, doi:10.1007/BF00877211.
Marone, C. (1998), Laboratory-derived friction laws and their application to seismic faulting, *Annu. Rev. Earth Planet. Sci.*, *26*, 643–696.
Marone, C., and C. H. Scholz (1988), The depth of seismic faulting and the upper transition from stable to unstable slip regimes, *Geophys. Res. Lett.*, *15*(6), 621–624, doi:10.1029/GL015i006p00621.
McKenzie, D., and J. N. Brune (1972), Melting on fault planes during large earthquakes, *Geophys. J. R. Astron. Soc.*, *29*, 65–78.
Mitchell, E., Y. Fialko, and K. Brown (2013), Temperature dependence of frictional healing of Westerly granite: Experimental observations and numerical simulations, *Geochem. Geophys. Geosyst.*, *14*, 567–582, doi:10.1029/2012gc004241.
Mitchell, E., Y. Fialko, and K. Brown (2015), Frictional properties of gabbro at conditions corresponding to slow slip events in subduction zones, *Geochem. Geophys. Geosyst.*, *16*, 4006–4020, doi:10.1002/2015GC006093.
Nagata, K., M. Nakatani, and S. Yoshida (2012), A revised rate- and state-dependent friction law obtained by constraining constitutive and evolution laws separately with laboratory data, *J. Geophys. Res.*, *117*, B02314, doi:10.1029/2011JB008818.
Nakatani, M. (2001), Conceptual and physical clarification of rate and state friction: Frictional sliding as a thermally activated rheology, *J. Geophys. Res.*, *106*(B7), 13,347–13,380.
Nathenson, M., and M. Guffanti (1988), Geothermal gradients in the conterminous United States, *J. Geophys. Res.*, *93*(B6), 6437–6450.
Nazareth, J. J., and E. Hauksson (2004), The seismogenic thickness of the southern California crust, *Bull. Seismol. Soc. Am.*, *94*(3), 940–960.
Newton, R. C. (1990), Fluids and shear zones in the deep crust, *Tectonophysics*, *182*(1), 21–37.
Niemeijer, A. R., and R. L. Vissers (2014), Earthquake rupture propagation inferred from the spatial distribution of fault rock frictional properties, *Earth Planet. Sci. Lett.*, *396*, 154–164.
Proctor, B., T. Mitchell, G. Hirth, D. Goldsby, F. Zorzi, J. Platt, and G. Di Toro (2014), Dynamic weakening of serpentinite gouges and bare surfaces at seismic slip rates, *J. Geophys. Res. Solid Earth*, *119*, 8107–8131, doi:10.1002/2014JB011057.
Reches, Z., and D. A. Lockner (2010), Fault weakening and earthquake instability by powder lubrication, *Nature*, *467*, 452–455, doi:10.1038/nature09348.
Rice, J. R. (2006), Heating and weakening of faults during earthquake slip, *J. Geophys. Res.*, *111*, B05311, doi:10.1029/2005JB004006.
Rice, J. R., N. Lapusta, and K. Ranjith (2001), Rate and state dependent friction and the stability of sliding between elastically deformable solids, *J. Mech. Phys. Solids*, *49*, 1865–1898.
Ruina, A. (1983), Slip instability and state variable friction laws, *J. Geophys. Res.*, *88*(B12), 10,359–10,370.
Saffer, D. M., and C. Marone (2003), Comparison of smectite-and illite-rich gouge frictional properties: Application to the updip limit of the seismogenic zone along subduction megathrusts, *Earth Planet. Sci. Lett.*, *215*(1), 219–235.
Sawai, M., A. R. Niemeijer, O. Plümper, T. Hirose, and C. J. Spiers (2016), Nucleation of frictional instability caused by fluid pressurization in subducted blueschist, *Geophys. Res. Lett.*, *43*, 2543–2551, doi:10.1002/2015GL067569.
Scholz, C. H. (2002), *The Mechanics of Earthquakes and Faulting*, 2nd ed., 496 pp., Cambidge Univ. Press, New York.
Shelly, D. R. (2010), Migrating tremors illuminate complex deformation beneath the seismogenic San Andreas Fault, *Nature*, *463*(7281), 648–652.

Sibson, R. H. (1973), Interaction between temperature and pore-fluid pressure during earthquake faulting—A mechanism for partial or total stress relief, *Nature*, *243*, 66–68.

Sibson, R. H. (1982), Fault zone models, heat flow, and the depth distribution of earthquakes in the continental crust of the United States, *Bull. Seismol. Soc. Am.*, *72*(1), 151–163.

Stesky, R. M. (1978), Mechanisms of high temperature frictional sliding in Westerly granite, *Can. J. Earth Sci.*, *15*(3), 361–375, doi:10.1139/e78-042.

Takeuchi, C., and Y. Fialko (2012), Dynamic models of interseismic deformation and stress transfer from plate motion to continental transform faults, *J. Geophys. Res.*, *117*, B05403, doi:10.1029/2011JB009056.

Trugman, D. T., C. Wu, R. A. Guyer, and P. A. Johnson (2015), Synchronous low frequency earthquakes and implications for deep San Andreas Fault slip, *Earth Planet. Sci. Lett.*, *424*, 132–139.

Tse, S. T., and J. R. Rice (1986), Crustal earthquake instability in relation to the depth variation of frictional slip properties, *J. Geophys. Res.*, *91*(B9), 9452–9472.

Tsutsumi, A., and T. Shimamoto (1997), High-velocity frictional properties of gabbro, *Geophys. Res. Lett.*, *24*, 699–702.

Wilson, C. K., C. H. Jones, P. Molnar, A. F. Sheehan, and O. S. Boyd (2004), Distributed deformation in the lower crust and upper mantle beneath a continental strike-slip fault zone: Marlborough fault system, South Island, New Zealand, *Geology*, *32*(10), 837–840.